Impact of land cover patch size on the accuracy of patch area representation in HNN-based super resolution mapping.

Muad, A. M. and Foody, G. M.

The manuscript of the above article revised after peer review and submitted to the journal for publication, follows. Please note that small changes may have been made after submission and the definitive version is that subsequently published as:

Impact of land cover patch size on the accuracy of patch area representation in HNN-based super resolution mapping.

Anuar M. Muad[1] and Giles M. Foody[2]

1. Department of Electrical, Electronic and Systems Engineering, Universiti Kebangsaan Malaysia, 43600 UKM Bangi, Selangor, Malaysia (e-mail: mikdad@eng.ukm.my)

2. School of Geography, University of Nottingham, Nottingham, NG7 2RD, UK (e-mail giles.foody@nottingham.ac.uk)

Abstract

Mixed pixels are one of the largest sources of error and uncertainty in mapping from remotely sensed data. A Hopfield neural network based approach to super-resolution mapping has become popular for mapping at a sub-pixel scale, partly because it seeks to maintain the class proportional information indicated by a soft classification analysis. The use of the approach is, however, handicapped by a lack of guidance on the parameter setting values and of the impacts of different landscape patterns on the analysis. Here, the sensitivity of the Hopfield neural network for super-resolution mapping is investigated with a focus on the effect of different landscape types and parameter settings using simulated and real data sets. It is shown that the method's suitability varies between landscapes, being most suited to situations in which landscape patches are large (>1 pixel). Additionally, for such landscapes the widely used scenario in which the weighting parameters are set at equal values is successful but the approach is less effective for the mapping of small isolated land cover patches. With the latter, it is shown to be important to weight the area constraint highly and undertake a large number of iterations. Critically, it is shown that equal weighted parameter settings and imbalanced settings to emphasise the area constraint are most suitable for landscapes comprising large and small patches respectively. Moreover, the positive attributes of these two sets of parameter settings may be combined to yield an enhanced mapping method for landscapes that comprise a mixture of patch sizes.

I. Introduction

Mixed pixels are one of the major sources of error and uncertainty in the mapping of land cover from remotely sensed data [1]. Given that a mixed pixel must by definition represent an area containing two or more land cover classes, such pixels cannot be appropriately represented by conventional 'hard' image classifications used widely to map land cover [2-4]. Unmixing and soft classification methods that allow for the multiple and partial class membership properties of mixed pixels have proved popular for mapping from remotely sensed imagery. They have been used in a range of studies, including those representing gradations between continuous classes [5,6] and those estimating the class composition of pixels [7,8] as well as forming the basis of important land cover data products such as vegetation continuous fields [9,10]. Although representing a major advancement on the conventional hard classification, the output of a soft classifier and its interpretation can be problematic. The output is, for example, typically a set of fraction images, each depicting the proportional cover of one of the classes in the area represented by the pixel which is harder to interpret than the standard, single layer, thematic map derived by a hard classification. Additionally, the soft classification only indicates the class composition of image pixels, it does not indicate the geographical distribution of the classes in the area represented by the pixels [11]. One means to address these concerns and produce a single layer land cover map which shows the spatial distribution of the classes at a finer resolution than the image is to apply a super resolution mapping technique to the output of a soft classification.

A variety of super resolution mapping methods has been used in remote sensing [11-18].One that has been widely promoted and demonstrates considerable potential is based on the Hopfield neural network (HNN) [19-21]. A key feature of the HNN is that it seeks to maintain the class proportional information of the soft classification in the super resolution map. Thus, the estimated proportion of a pixel's area comprised of a class depicted in a soft classification, or a value close to it, should also be contained in the same region in the output of the super-resolution mapping analysis.

With the HNN based approach to super-resolution mapping, a pixel is decomposed into a large number of sub-pixels and the class labels of these sub-pixels are distributed in proportion to the class composition information provided by a soft classification for the pixel. The labels are initially distributed randomly amongst the sub-pixels and the HNN estimates their spatial distribution through an iterative analysis. The latter involves adjusting the sub-pixel class labels on the basis of the class label information for a sub-pixel and its immediate neighbourhood. As the approach incorporates spatial context into the determination of the location of sub-pixel class fractions the method is most suitable for the scenario in which the land cover patches are relatively large relation to the image pixel size. This type of scenario is common, with mixed pixels occurring at the edge of patches. There is, however, a variety of land cover mixing scenarios [22] and the basic HNN approach may not always be appropriate for the representation of the land cover distribution. In particular, one concern is when the mixing arises because of the landscape mosaic comprises small (area <1 pixel) isolated land cover patches. This may be a common occurrence, with the amount of small land cover patches varying as an interactive function of patch size relative to image spatial resolution.

This article aims to evaluate the effect of land cover patch size on the accuracy of super resolution mapping by a HNN with particular regard to the accuracy with which patch area is represented. Section II provides a review of the key features of the HNN algorithm used for super resolution mapping. The data and methods used are described in Section III. Section IV provides the results and section V the conclusions.

II. HNN

The HNN is a recurrent artificial neural network which is designed for the solution of optimization problems [23, 24]. The fundamental structure of the network consists of a single layer of neurons and the output of each neuron is fed back to all other neurons except itself. The HNN is an optimization tool defined by an energy function [24] formulated for the application. In super-resolution mapping applications, each pixel of a coarse spatial resolution image is typically sub-divided into $z \times z$ sub-

pixels, where z is the zoom or scale factor of the spatial resolution increment. Each sub-pixel is associated with a single neuron in the HNN and can be located by its coordinates in the sub-pixel grid. The input to the neuron at row i column j of the grid is u_{ij} and its output is v_{ij}.

The energy function that represents the problem of super-resolution mapping is generally represented as the sum of a goal and constraint term. The goal function considers the spatial correlation between observations, working on a neuron together with its closest neighbours rather than treating each neuron as an independent unit. The constraints specify the context of the available data by adding costs to the objective. By assuming that the spatial dependence between a neuron and its adjacent neurons is larger than that of neurons that are more distant, the energy function can be represented as the combination of spatial clustering goal functions and an area proportion constraint [19, 20, 25] which can be expressed as

$$E = -\sum_i \sum_j \left(k_1 G_{ij}^{ON} + k_2 G_{ij}^{OFF} + k_P P_{ij} \right) \tag{1}$$

where E is the network energy, G_{ij}^{ON} and G_{ij}^{OFF} are the goal functions at a neuron (i, j), P_{ij} is the area proportion constraint, k_1, k_2, and k_P are the weight constant for the goal functions and the area proportion constraint respectively. The rate of change for the energy function for a neuron is

$$\frac{dE_{ij}}{dv_{ij}} = k_1 \frac{dG_{ij}^{ON}}{dv_{ij}} + k_2 \frac{dG_{ij}^{OFF}}{dv_{ij}} + k_P \frac{dP_{ij}}{dv_{ij}} \tag{2}$$

The goal functions maximize the spatial correlation of nearby neurons that have similar values. The functions receive input from the neuron and its eight surrounding neurons. Two goal functions are used to drive the output into two binary states: on and off. The first goal function, G^{ON}, increases the output of a neuron to 1 if the average value of its eight surrounding neurons is greater than a threshold value, $T=0.5$. If the average of the surrounding neurons is less than the threshold value, the goal

function becomes 0. This function makes the output of a neuron similar to that of its neighbouring

neurons and is based on

$$\frac{dG_{ij}^{ON}}{dv_{ij}} = \frac{1}{2}\left[1 + \tanh\left(\frac{1}{8}\sum_{\substack{k=i-1 \\ k \neq i}}^{i+1}\sum_{\substack{l=j-1 \\ l \neq j}}^{j+1} v_{kl} - T\right)\lambda\right] \times \left(v_{ij} - 1\right) \tag{3}$$

where λ is the gain that determines the steepness of the tanh function. The second goal

function, G_{ij}^{OFF}, decreases the output of a neuron to 0 if the average value of its eight surrounding

neurons is less than T. If the average of the surrounding neurons is greater than T, the second function

increases the output of the centre neuron to 1. Again, this function makes the output of a neuron

similar to that of its neighbouring neurons and is based on

$$\frac{dG_{ij}^{OFF}}{dv_{ij}} = \frac{1}{2}\left[1 - \tanh\left(\frac{1}{8}\sum_{\substack{k=i-1 \\ k \neq i}}^{i+1}\sum_{\substack{l=j-1 \\ l \neq j}}^{j+1} v_{kl} - T\right)\lambda\right] \times v_{ij} \tag{4}$$

The area proportion constraint regulates the energy equation by seeking to retain the pixel class

proportion derived from soft classification, which for a pixel at location (x,y) in the image's pixel grid

is denoted a_{xy}. The area proportion constraint is based on

$$\frac{dP_{ij}}{dv_{ij}} = \left(\frac{1}{2z^2}\sum_{m=xz}^{xz+z-1}\sum_{n=yz}^{yz+z-1}\left(1 + \tanh\left(v_{mn} - T\right)\lambda\right)\right) - a_{xy} \tag{5}$$

If the area proportion of the estimate for the original pixel is lower or greater than the target area, the

output values of the neurons are increased or decreased accordingly to help address the problem [19,

25]. The value for each neuron in the HNN can be updated numerically using a Euler method [26] and

is expressed as

$$u_{ij}(t + \Delta t) = u_{ij}(t) + \frac{du_{ij}(t)}{dt} \Delta t \qquad (6)$$

which advances a solution from state $u_{ij}(t)$ to state $u_{ij}(t + \Delta t)$ with Δt as time step [19,25].

Equation 6 runs iteratively until $\sum_{ij}\left(u_{ij}(t + \Delta t) - u_{ij}(t)\right) \le \varepsilon$, where ε is a small value.

Operational use of the HNN approach to super-resolution mapping requires the analyst to specify the values of the weight parameters in equation 1 and the number of iterations to undertake or value for ε to act as a stopping criterion. The selection of optimum parameter settings can be a difficult and tedious process and the literature provides little guidance on the settings to use. It is common, for example, for weighting parameters to be set at equal values and to use >2000 iterations [19, 25]. The settings used are often selected on the basis of assumptions made by the analyst and trial runs [19, 21]. A strategy to enhance the analysis is also to include prior information on the land cover mosaic, if known, perhaps via a semi-variance function [21] and/or provision of ancillary data [27, 28]. The inclusion of prior information in terms of a semi-variance function is, for example, one means to enhance the utility of the HNN for the representation of small land cover patches. To achieve this, the basic approach represented by equation 1 is adjusted such that the energy function is represented as the sum of a set of semi-variance functions and an area proportion constraint [21] which, assuming a zoom of z, can be expressed as

$$E = -\sum_i \sum_j \left(k_1 S_{ij}^{(1)} + k_2 S_{ij}^{(2)} + \cdots + k_z S_{ij}^{(z)} + k_P P_{ij}\right) \qquad (7)$$

where k_1 to k_z are weighting factors for the output values for z^{th} semi-variance function, $S_{ij}^{(1)}$ to $S_{ij}^{(z)}$. As explained by [21] the rate of change for the energy function becomes

$$\frac{dE_{ij}}{dv_{ij}} = \left(\sum_{n=1}^{z} k_n \frac{dS_{ij}^{(n)}}{dv_{ij}}\right) + k_P \frac{dP_{ij}}{dv_{ij}} \qquad (8)$$

in which the first part corresponds to the semi-variance functions while the second part is for

the area proportion constraint. The prior knowledge about spatial pattern, perhaps from a fine

spatial resolution image, is modelled using a semi-variance function

$$\gamma(h) = \frac{1}{2N(h)} \sum_{i=1, j=1}^{N(h)} \left(f_{ij} - f_{i\pm h, j\pm h} \right)^2 \qquad (9)$$

in which $\gamma(h)$ is the semi-variance at lag h, $N(h)$ is the number of pixels at lag h from the

centre pixel (i,j) and f_{ij} is a pixel of the fine spatial resolution image used to generate the prior

information. Further details on the approach are given in [21].

III. Data and Methods

A variety of real and simulated data sets were used and discussed in four groupings.

A. Fine resolution imagery

To illustrate the sensitivity of the HNN to different mixing scenarios a set of four small images

representing similar land covers but present in different patterns was derived from a SPOT image

contained in Google Earth for a site near Granada, Spain. Each image extract was derived from a

region lying between latitudes 37° 08' 19"N and 37° 07' 41"N and longitudes 4° 07' 60"W and 4° 07'

09"W from an image acquired on 1 October 2004. The agricultural land use of the site produced four

visually different landscape patterns, A-D (Figure 1) each comprised of two classes: vegetation and its

background. Each image was spatially degraded by a factor of 8 with the pixels in the derived

simulated coarse resolution images taking on the average value of the pixels in an 8×8 area of the

original image. These simulated coarse resolution images were subjected to a series of analyses, using

a standard *k*-means hard classification and super-resolution mapping by HNN using a zoom factor of

8 to predict the land cover distribution. The number of cluster in the *k*-means classifier was set to two

to differentiate between the vegetation and its background. The input to the HNN analyses was a soft

classification of the coarse resolution images derived from the use of a fuzzy *c*-means (FCM; [29])

classifier in which the weighting parameter that determines the degree of fuzziness was set to 2.0. Following common practice, the weights in the HNN were set to equal values: $k_1=k_2=k_p=1$. A further analysis was undertaken with the HNN informed by information on the land cover pattern represented by the semi-variogram [21] derived from each of the original resolution images.

Accuracy assessment is typically based on the comparison of the derived land cover representation against a high quality reference. As a gold-standard reference data set is typically unavailable, this process often involves the evaluation of the degree of agreement between the derived representation and another, high quality, classification used as a reference [1]. Here, the accuracy of each analysis was evaluated against a standard hard classification of the relevant original fine resolution imagery (Figure 1c). The latter reference data were derived by a k-means classification of the original imagery. The degree of correspondence between the predicted and ground reference land cover distributions was evaluated visually and by cross-tabulation of the pixel labels, at a sub-pixel scale, with accuracy expressed as the percentage overall agreement in labelling. Although there are concerns with the use of site-specific accuracy assessment in the evaluation of super-resolution maps [30] the focus here is on the relative rather absolute magnitude of the estimates derived.

B. Simulated blocks of pixels

The relationship between land cover patch size and its predicted area was explored with simulated data representing blocks of image pixels. As with the previous example, the focus was on a simple situation in which there are just two classes; the patch and its background. Initial analyses focused on the representation of a relatively large patch and a small isolated patch by the standard HNN. This situation was evaluated with simulated data comprising blocks of 3×3 pixels in a coarse spatial resolution image. Two sets of scenarios were evaluated. The first was for the situation when the land cover patches were relatively large and information from neighbouring pixels could usefully inform the HNN analysis and the soft classification value of the central pixel was varied from 0.05 to 1.0 with all values at a 0.05 step evaluated. The second set of scenarios was similar but with the land cover patch to be represented being small and isolated. In this instance only the central pixel in the

block contains a single small patch of one land cover class with the rest of the 3×3 pixel area representing the background class. Again the soft classification value of the central pixel was varied over the range 0.05 to 1.0. In each case it was assumed that the soft classification of the data was perfect, and so the DN or value for a pixel in the soft classified image corresponded to the proportional cover of the class in the area represented by that pixel.

Three different HNNs were evaluated. First, the weighting parameters were set at equal values. Specifically, the $k_1=k_2=k_p=1$ scenario was again used and as the parameters were of equal magnitude this is approach is referred to as HNN(E). Second, a HNN with the goal function parameters set at a higher level than the area proportion constraint. This latter analysis used $k_1=k_2=1.0$ and $k_p=0.1$ and as the goal functions were emphasised is referred to as HNN(G). Thirdly, a scenario in which the area proportion constraint was emphasised over the goal functions. With this scenario $k_1=k_2=0.1$ and $k_p=1.0$ and as the area proportion constraint was emphasised it is referred to as HNN(A). Analyses with these three HNNs were undertaken over a range of iterations: 1,000, 2,000, 5,000, 10,000 and 15,000.

To further explore the effects of different weight parameter settings, the HNN(G) approach was also modified to explore the effect of variation in the k_p value. For this, $k_1=k_2=1.0$ throughout but the value of k_p was altered in 0.1 increments over the range 0.1 to 1.0. Similarly, with the HNN(A) approach a series of analyses were undertaken in which k_p was fixed at 1.0 throughout but the value for $k_1=k_2$ was varied over the range 0.1 to 1.0 with a 0.1 step.

C. Simulated imagery

Variation in the representation of patch area was expected, mainly because the relative weighting of the area proportion constraint in the various analyses. It was anticipated that the accuracy of patch representation derived with the data outlined in section B above would vary between the three HNN scenarios as a function of patch size. However, it was also anticipated that the strengths of different approaches could be exploited and combined to form an enhanced analysis. To assess this, an image containing 34 patches of variable size was generated manually (Figure 2a); the size and location of the

patches was determined in an unplanned, haphazard, manner. As with other analyses, this image was degraded by a factor of 8 and a soft classification of the resulting coarse resolution image derived by the FCM with the weighting parameter set to 2.0. The soft classification was used as input to the HNN(E) and HNN(A). The outputs of these HNNs were also combined. This was achieved by using the output of HNN(E) for the large patches (defined here as >1 pixel in area) and HNN(A) for the remaining, small, patches. Since the approach is a combination of two HNN scenarios this is referred to later as the HNN2.

The area of the patch in the output of each HNN analysis was calculated by counting the number of sub-pixels allocated to the patch class. This value could be compared directly against the actual proportion of patch cover, which was known from the simulation. Attention focused on the accuracy of the estimation over a range of patch sizes, expressed in terms of the patch proportional cover, which is illustrated in plots of the predicted against actual cover. In these plots deviation from the 1:1 line indicates error, with values lying below the line highlighting an underestimation of patch area.

D. Coarse resolution imagery

Finally, a series of analyses of remote sensor data sets were undertaken to illustrate the issues in a real application. As in other studies, the adoption of finer spatial resolution imagery can enhance spatial detail and provide accurate information [31, 32]. Here, the focus was on the mapping of high latitude lakes from MODIS imagery. Presently there is considerable uncertainty over the number and size of lakes [33], especially at high latitudes where they may be disappearing due to climate change [34]. Mapping and monitoring lakes over such large regions is realistically only feasible with moderate spatial resolution systems such as MODIS, but the spatial resolution makes it difficult to study small lakes, which are often of interest as associated with considerable uncertainty [33]. Here, the potential of HNN based super-resolution mapping for the provision of information on lakes was evaluated. This work mapped lakes from MODIS data for a test site in Quebec province of Canada (Figure 3) acquired on 5 July 2002. As attention was focused on mapping water, which is relatively separable from land in the near-infrared part of the spectrum, and especially small lakes, a 250m spatial

resolution image in the near infrared (841-876 nm) waveband was used. The MODIS imagery used

was derived from tile 13 horizontal and 03 vertical of the MOD09GQ, a level 2 data, which have not

been gridded into a map projection as in Level 3 data of composite images [35], facilitating further

processing to be determined by users, such as relative shift measurement and reduction of sensor point

spread function effects [36]. The MODIS images were projected from Sinusoidal projection into a

Landsat Universal Transverse Mercator (UTM) projection at zone 16.

A Landsat ETM+ image with a 30m spatial resolution acquired five days after the MODIS image on

10 July 2002 was also obtained. The image used was acquired on path 25 row 22 and obtained from

the US Geological Survey. A k-means hard classification of the ETM+ data acquired in the near-

infrared waveband (770-900nm) was used as reference data for the evaluation of the analyses of the

MODIS data. The latter analyses included a standard k-means hard classification and super-resolution

mapping using the HNN(E) and HNN(A), both with $z=8$ and run for 10,000 iterations. Note that the

settings of the HNN analyses yield a map with a spatial resolution of ~31.2 m, approximately the

same as the ETM+ data used as reference data. As previously, the FCM with a weighting parameter of

2.0 was used to generate a soft classification for input to the HNN.

IV. Results and Discussion

A. Fine resolution imagery

The four landscape mosaics, A-D (Figure 1), were represented with varying quality by the k-means

hard classification and HNN analyses. For each landscape, the hard classification provided the least

accurate representation which was also unrealistic visually due to its blocky nature (Figure 1d). The

hard classification was particularly poor in representing mosaic B, with many of the very small, sub-

pixel sized, patches not represented in the classified image. The accuracy with which the four

landscapes were mapped by the hard classification ranged from 73.52% to 81.86%

The super-resolution maps were all more accurate than the hard classification for each landscape type

(Figure 1). There was, however, considerable variation in the quality of the representations derived.

For example, with the basic HNN (figure 1e), landscape A was classified to a very high accuracy, and substantially higher than the representation derived for that landscape in the hard classification. For landscape B, however, the HNN was only marginally (0.25%) more accurate than that observed with the hard classification. The accuracy of the HNN derived maps varied from 73.77% to 91.79%, a range of 18.02%, a result which highlights that the utility of the HNN for super-resolution mapping varies as a function of the landscape mosaic to be represented.

The addition of prior information into the HNN analysis increased the accuracy of the land cover representations for all four landscapes. Accuracy varied from 88.73% for landscape B to 96.70% for landscape A, a range of 7.97% (Figure 1f). The acquisition of suitable prior information may, however, be difficult. Furthermore, it is important that the prior information used is suitable. Figure 4 illustrates the effect of using an inappropriate prior on the analysis, with the output over-influenced by the prior.

The analyses of the four landscapes (Figure 1) highlight the value of super-resolution mapping over conventional hard classification. More critically, they also show that the HNN based approach varies in suitability over the four landscapes, being most suitable when the patches were relatively large (e.g. landscape A) and least where the patches were small (e.g. landscape B). The impact of variation in patch size on the HNN was explored further with the simulated data.

B. Simulated blocks of pixels

The impact of land cover patch size on the super-resolution representation is illustrated in Figures 5-8. For large patches, the basic HNN approach produced a visually realistic representation of the geographical distribution of the classes. In Figures 5 and 6 it is evident how information from neighbouring pixels aided the location of the patch cover in the central pixel. However, for small patches, which are associated with a low value in the soft classification and surrounded by other low or zero values, the HNN can produce a reasonable representation if the patch is relatively large (Figure 7) but not if it is small (Figure 8). This simple illustration shows the effect of the magnitude of

the soft classification value of a pixel and its neighbours on the prediction of land cover distribution by HNN.

In the basic HNN approach the algorithm's parameters had, as is common practice, been set at equal values ($k_1=k_2=k_p=1$). Varying the parameter values may be one means to enhance the representation, especially of the small patches that have been shown above to be problematic in super-resolution mapping by HNN.

Using the HNN(E), HNN(G) and HNN(A), the analyses reported above were repeated but across the full range of soft classification values. For large land cover patches each of the three HNN scenarios provided accurate representations of the patch area, with predictions lying close to the 1:1 line in Figure 9a. Differences between the scenarios were small but most apparent at low soft classification values. The results indicated that the minimum soft classification value, and so patch size, required for a patch to be represented in the output was 0.05 for HNN(G), 0.15 for HNN(A) and 0.20 for HNN(E); the estimated size of these patches were close to the 1:1 line across the full range of soft classification values above the minimum patch size noted.

For the small patches, however, it was evident that the accuracy with which patch size was estimated by all three HNN scenarios varied greatly with the soft classification value and hence patch size (Figure 9b). It was especially evident that while HNN(A) consistently underestimated patch size the estimates derived were close to the actual value, lying close to the 1:1 line. However, the results from the HNN(E) and, especially, HNN(G) were less accurate. For the HNN(E) patch size was again consistently underestimated but generally close to the 1:1 line for soft classification values >0.5. At a soft classification value <0.5 the underestimation was large and a patch was not represented at all at values of 0.4 and below. The HNN(G) provided the least accurate results for small patches. Again, patch size was consistently underestimated, deviating considerably from the 1:1 line across the entire range of soft classification values. Additionally, a patch associated with a soft classification value of 0.55 or smaller would not be represented in its output. It was evident, therefore, that for small patches

the HNN(A) was able to provide accurate predictions of patch size across the entire range of soft classification values, helping to address concerns highlighted in relation to Figure 8. The HNN(E) and HNN(G) were less useful, especially for the smallest patches.

As well as the values of the k_1, k_2 and k_p weighting parameters, the number of iterations can have an impact on super-resolution mapping by a HNN. Variation in the number of iterations had little effect on the representation of the large land cover patches by the three HNN scenarios except for the HNN(A) (Figure 10). With the latter, it was evident that at a small number of iterations, 2000 or less, poor estimates of patch size were derived. For large land cover patches the HNN(E) and HNN(G) could be used to derive accurate estimates with a small number of iterations. A larger number of iterations, here ~5000 or more, was required for accurate estimation with the HNN(A).

For the small land cover patches the number of iterations had little impact on the accuracy of the estimates derived from the HNN(E) and HNN(G) but a large effect on the results from the HNN(A) (Figure 11). With the latter, the estimates derived from the use of 2000 and especially 1000 iterations were substantially underestimated. However, with a large number of iterations, the accuracy was high with estimates lying close to the 1:1 line (Figure 11). This is further emphasised in the visualization in Figure 12 of the results for one of the analyses, based on the situation when the value of the pixel in the soft classification was 0.2, which shows the requirement for a large number of iterations. The results above highlight the potential of the HNN(A) for the representation of small land cover patches, especially when a relatively large number of iterations is used.

As the weight parameter settings used in the scenarios were defined relatively arbitrarily, it is interesting to note results obtained from different settings as this could influence the performance of the HNN(G) and HNN(A) methods. With the HNN(G) it was apparent that with $k_1=k_2=1$ variation in k_p greatly influenced the accuracy of the patch size estimation (Figure 13). Critically, it was evident that the most accurate estimates were derived with large k_p. With the HNN(A), if the value of k_p was kept at 1 it was evident that the accuracy of the patch size estimation varied with the value of k_1 and

k_2. In particular, when the soft classification value was low a small value for k_1 and k_2 was preferable (Figure 14).

The results indicate that HNN(E) is suited to the situation when the patches are large, larger than a pixel. For patches smaller than the size of the pixel, the HNN(A) was most suitable, especially if low values were used for k_1 and k_2 and large number of iterations undertaken.

C. Simulated imagery

Application of the HNN(E) and HNN(A) approaches to a simulated image containing a variety of patches of differing size helps illustrate their potential and limitations for super-resolution mapping. Of the 34 patches present (figure 2a), the HNN(E) was able to represent only 4 large patches (Figure 2c). Alternatively, the HNN(A) was more suited to the task as most patches were small and isolated and so it was able to represent 24 of the patches (Figure 2d); the 10 patches it missed were typically very small. However, it was evident that the representation of the large patches by the HNN(A) was often poor, with size and shape visually incorrect (Figure 2d).

The results highlight that the HNN(E) may be expected to work well for large patches while the HNN(A) appears most suitable for the representation of small patches. In many landscapes there may be a mixture of patch sizes and neither approach would be ideal. The proposed HNN2 approach, which seeks to use the positive aspects of each method by gaining information on the large patches from the HNN(E) and the small patches from HNN(A) provided a better representation than the two HNNs it was based on. It too yielded a representation of 24 patches (Figure 2e) but visually this was superior to that from both the HNN(E) and HNN(A).

D. Coarse resolution imagery

Similar trends were also observed in the analyses based on the MODIS data. The test site contained a wide variety of lakes, differing greatly in terms of size and shape. Critically, some of the lakes were relatively large in relation to the pixel size, and so suited to standard HNN(E) analysis, while many

were small and isolated and not suited to standard HNN analyses. A visual analysis illustrates the quality of the mapping by standard hard classification and HNN based methods (Figure 15). The hard classification of the MODIS data yielded a representation in which the lake boundaries were unrealistically jagged and clearly omitted the numerous small lakes (Figure 15b). The soft classification of the MODIS image yielded an enhanced representation (Figure 15c), with information on the small lakes more apparent. However, the three HNN analyses based on the soft classification provided representations that were much closer to the reference data than the standard hard classification. As noted above, the reference data set was a k-means classification of the Landsat ETM+ data. While it is not feasible to provide a rigorous evaluation of the accuracy of the k-means classification and so its suitability as a reference, a guide to its quality was obtained by checking its labelling against visual interpretation of the Landsat ETM+ image. The latter indicated that the k-means classification had an accuracy of 90.5% and so provides a strong, albeit imperfect, reference data set.

It was evident that the HNN(E) appeared to provide an accurate representation of the large lakes, with small lakes omitted (Figure 15d). The HNN(A) and HNN2, however, provided representations that depicted a greater number and variety of lakes (Figure 15e, 15f). While not suited to site-specific accuracy assessment because the precise location of a small patch is uncertain [30], non-site specific accuracy assessment highlighted some important trends. The reference data indicated that the total extent of lake water in the region was 202.09 km^2, with much of this area associated with small, often very small, lakes. The HNN(E) which omitted small lakes provided a representation with 151.89 km^2 while the HNN(A) and HNN2 were closer with 161.94 km^2 and 162.89 km^2. Although there was little difference between the HNN(A) and HNN2 in terms of the areal extent estimates, it was apparent that the shape of the lakes appeared to be more accurately represented by the HNN2. Further work to validate these and other super-resolution products would be useful but needs to address concerns linked to the required precision in the mapping.

V. Conclusions

The HNN has been widely used in super-resolution mapping applications. One attraction of the approach is that it includes a parameter that seeks to maintain the class proportional information provided by the soft classification upon which the analysis is based. There is, however, little guidance in the literature on what weight settings to use and the suitability of the HNN for different types of landscape. Here, the effect of different parameter settings and landscape patterns on HNN analysis was evaluated. There are five main conclusions to this work:

1. The suitability of the HNN for super-resolution mapping varies as a function of the landscape to be represented. The basic HNN approach with equally weighted parameters, HNN(E), was able to provide accurate representations when patches were large but not when small. For example, the accuracy with which a landscape comprising relatively large patches was increased from 79.86% with a hard classification to 91.79% with the HNN(E). However, for a landscape composed of small patches the accuracy of the representation derived from a hard classification and HNN(E) analysis were very similar, at 73.52% and 73.77% respectively.

2. The incorporation of prior information into the HNN analysis could increase the accuracy of the mapping for each landscape pattern but it was essential that an appropriate prior was used.

3. When patches were relatively large, all three HNN scenarios investigated were able to derive highly accurate land cover representations. Additionally, the number of iterations had little effect on the results of the HNN mapping except for the HNN(A) which yielded most accurate representations when a large number of iterations was used.

4. When patches were relatively small, the HNNs using equally weighted and goal emphasised parameter settings tended to underestimate patch area, especially for the very small patches. By emphasising the area proportion constraint, as in HNN(A), the accuracy with which small patches could be represented was increased, especially if a large number of iterations was employed. Critically, the popular use of equal parameter values in the HNN(E) yielded substantial under-estimation of patch area when patch size was <0.5 pixel area.

5. When the region to be mapped contains a variety of patch sizes, both large and small, neither the HNN(E) or HNN(A) approach is ideal. However, the output of the HNN(E) may be used

to represent large patches and combined with that from HNN(A) for small patches to derive an enhanced representation.

References

1. G. M. Foody, "Status of land cover classification accuracy assessment," *Remote Sensing of Environment*," vol. 80, pp. 185-201, 2002.

2. P. F. Fisher and S. Pathirana, "The evaluation of fuzzy membership of land cover classes in the suburban zone", *Remote Sensing of Environment*, vol. 34, pp. 121-132, 1990.

3. G. M. Foody, "Approaches for the production and evaluation of fuzzy land cover classifications from remotely-sensed data," *International Journal of Remote Sensing*, vol. 17, pp. 1317-1340, 1996.

4. F. Wang, "Fuzzy supervised classification of remote-sensing images", *IEEE Transactions on Geoscience and Remote Sensing*, vol. 28, pp. 194-201, 1990.

5. T. F. Wood and G. M. Foody, "Analysis and representation of vegetation continua from Landsat Thematic Mapper data for lowland heaths," *International Journal of Remote Sensing*, vol. 10, pp. 181-191, 1989.

6. G. M. Foody, N. A. Campbell, N. M. Trodd, and T. F. Wood, "Derivation and applications of probabilistic measures of class membership from the maximum-likelihood classification, *Photogrammetric Engineering and Remote Sensing*, vol. 58, pp. 1335-1341, 1992.

7. J. Knight and M. Voth, "Mapping impervious cover using multi-temporal MODIS NDVI data", *IEEE Journal of Selected Topics in Applied Earth Observations and Remote Sensing*, vol. 4, pp. 303-309, 2011.

8. S. Lee and R. G. Lathrop, "Subpixel analysis of Landsat ETM+ using self-organising map (SOM) neural networks for urban land cover characterization, *IEEE Transactions on Geoscience and Remote Sensing*, vol. 44, pp. 1642-1654, 2006.

9. R. S. Defries, M. C. Hansen and J. R. G. Townshend, "Global continuous fields of vegetation characteristics: a linear mixture model applied to multi-year 8 km AVHRR data," *International Journal of Remote Sensing*, vol. 21, pp. 1389-1414, 2000.

10. M. C. Hansen, A. Egorov, D. P. Roy, P. Potapov, J. C. Ju, S. Turubanova, I. Kommareddy and T. R. Loveland, "Continuous fields of land cover for the conterminous United States using Landsat data: first results from the Web-Enabled Landsat Data (WELD) project,", *Remote Sensing Letters*, vol. 2, pp. 279-288, 2011.

11. A. M. Muslim, G, M. Foody and P. M. Atkinson, "Shoreline mapping from coarse-spatial resolution remote sensing imagery of Seberang Takir, Malaysia, *Journal of Coastal Research*, vol. 23, pp. 1399-1408, 2007.

12. K. C. Mertens, L. P. C. Verbeke, T. Westra and R. R. De Wulf, "Sub-pixel mapping and sub-pixel sharpening using neural network predicted wavelet coefficients," *Remote Sensing of Environment*, vol. 91, pp. 225-236, 2004.

13. A. Boucher, P. C. Kyriakidis and C. Cronkite-Ratcliff, "Geostatistical solutions for super-resolution land cover mapping," *IEEE Transactions on Geoscience and Remote Sensing*, vol. 46, pp. 272-283, 2008.

14. Z. Shen, J. Qi and K. Wang, "Modification of pixel-swapping algorithm with initialization from a sub-pixel/pixel spatial attraction model," *Photogrammetric Engineering and Remote Sensing*, vol. 75, pp. 557-567, 2009.

15. Y. Ge, S. Li, V. C. Lakhan, "Development and testing of a subpixel mapping algorithm," *IEEE Transactions on Geoscience and Remote Sensing*, vol. 47, pp. 2155-2164, 2009.

16. A. Villa, J. Chanussot, J. A. Benediktsson and C. Jutten, "Spectral unmixing for the classification of hyperspectral images at a finer spatial resolution,", *IEEE Journal of Selected Topics in Signal Processing*, vol. 5, pp. 521-533, 2011.

17. A. M. Muad and G. M. Foody, "Super-resolution mapping of lakes from imagery with a coarse spatial and fine temporal resolution," *International Journal of Applied Earth Observation and Geoinformation*, vol. 15, pp. 79-91, 2012.

18. X. Li, T. X. Zhao and X. Chen, "A super resolution approach for spectral unmixing of remote sensing images," *International Journal of Remote Sensing*, vol. 32, pp. 6091-6107, 2011.

19. A. J. Tatem, H. G. Lewis, P. M. Atkinson, and M. S. Nixon, "Super-resolution target identification from remotely sensed images using a Hopfield neural network," *IEEE Transactions on Geoscience and Remote Sensing*, vol. 39, pp. 781-796, 2001.

20. A. J. Tatem, H. G. Lewis, P. M. Atkinson, and M. S. Nixon, "Multiple-class land-cover mapping at the sub-pixel scale using a Hopfield neural network*," International Journal of Applied Earth Observation and Geoinformation*, vol. 3, pp. 184-190, 2001.

21. A. J. Tatem, H. G. Lewis, P. M. Atkinson, and M. S. Nixon, "Super-resolution land cover pattern prediction using a Hopfield neural network," *Remote Sensing of Environment*, vol. 79, pp. 1-14, 2002.

22. P. Fisher, "The pixel: a snare or a delusion," *International Journal of Remote Sensing*, vol. 18, pp. 679-685, 1997.

23. J. J. Hopfield, "Neural networks and physical systems with emergent collective computational abilities," *Proceedings of the National Academy of Sciences*, USA, vol. 79, pp. 2554-2558, 1982.

24. J. J. Hopfield, "Neurons with graded response have collective computational properties like those of two-state neurons," *Proceedings of the National Academy of Sciences*, USA, vol. 81, pp. 3088-3092, 1984.

25. F. Ling, Y. Du, F. Xiao, H. Xue and S. Wu, S. "Super-resolution land-cover mapping using multiple sub-pixel shifted remotely sensed images," *International Journal of Remote Sensing*, vol. 31, pp. 5023-5040, 2010.

26. W. H. Press, S. A. Teukolsky, W. T. Vetterling and B. P. Flannery, *Numerical Recipes: The Art of Scientific Computing*, 3rd ed. Cambridge University Press, Cambridge, 2007.

27. Q. M. Nguyen, P. M. Atkinson and H. G. Lewis, "Superresolution mapping using a Hopfield neural network with LiDAR data," *IEEE Geoscience and Remote Sensing Letters*, vol. 2, pp. 366-370, 2005.

28. Q. M. Nguyen, P. M. Atkinson and H. G. Lewis, "Super-resolution mapping using Hopfield neural network with panchromatic imagery," *International Journal of Remote Sensing*, vol. 32, pp. 6149-6176, 2011.

29. J. C. Bezdek, R. Ehrlich and W. Full, "FCM: The fuzzy c-means clustering algorithm," *Computers and Geosciences*, vol. 10, pp. 191-203, 1984.

30. A. M. Muad, "*Super resolution mapping*", Unpublished PhD thesis, University of Nottingham, August 2011.

31. M. F. McCabe, P. Chylek and M. K. Dubey, "Detecting ice-sheet melt area over western Greenland using MODIS and AMSR-E data for the summer periods of 2002-2006," *Remote Sensing Letters*, vol. 2, pp. 117-126, 2011.

32. Y. H. He, S. E. Franklin, X. L. Guo and G. B. Stenhouse, "Object-orientated classification of multi-resolution images for the extraction of narrow linear forest disturbance," *Remote Sensing Letters*, vol. 2, pp. 147-155, 2011.

.

33. J. A. Downing, Y. T. P. Striegl, W. H. McDowell, P. Kortelainen, N. F. Caraco, J. M. Melack and J. J. Middelburg, The global abundance and size distribution of lakes, ponds and impoundments," *Limnanography and Oceanography*, vol, 51, pp. 2388-2397, 2006.

34. L. C. Smith, Y. Sheng, G. M. MacDonald and L. D. Hinzman, L. D. "Disappearing artic lakes," *Science*, vol. 308, pp. 1429, 2005.

35. E. F. Vermote, N. Z. El Saleous and C. O. Justice, "Atmospheric correction of MODIS data in the visible to middle-infrared: first results", *Remote Sensing of Environment*, vol. 83, pp. 97-111, 2002.

36. C. J. Jackett, P. J. Turner, J. L. Lovell, and R. N. Williams, "Deconvolution of MODIS imagery using multiscale maximum entropy," *Remote Sensing Letters*, vol. 2, pp. 179-187, 2011.
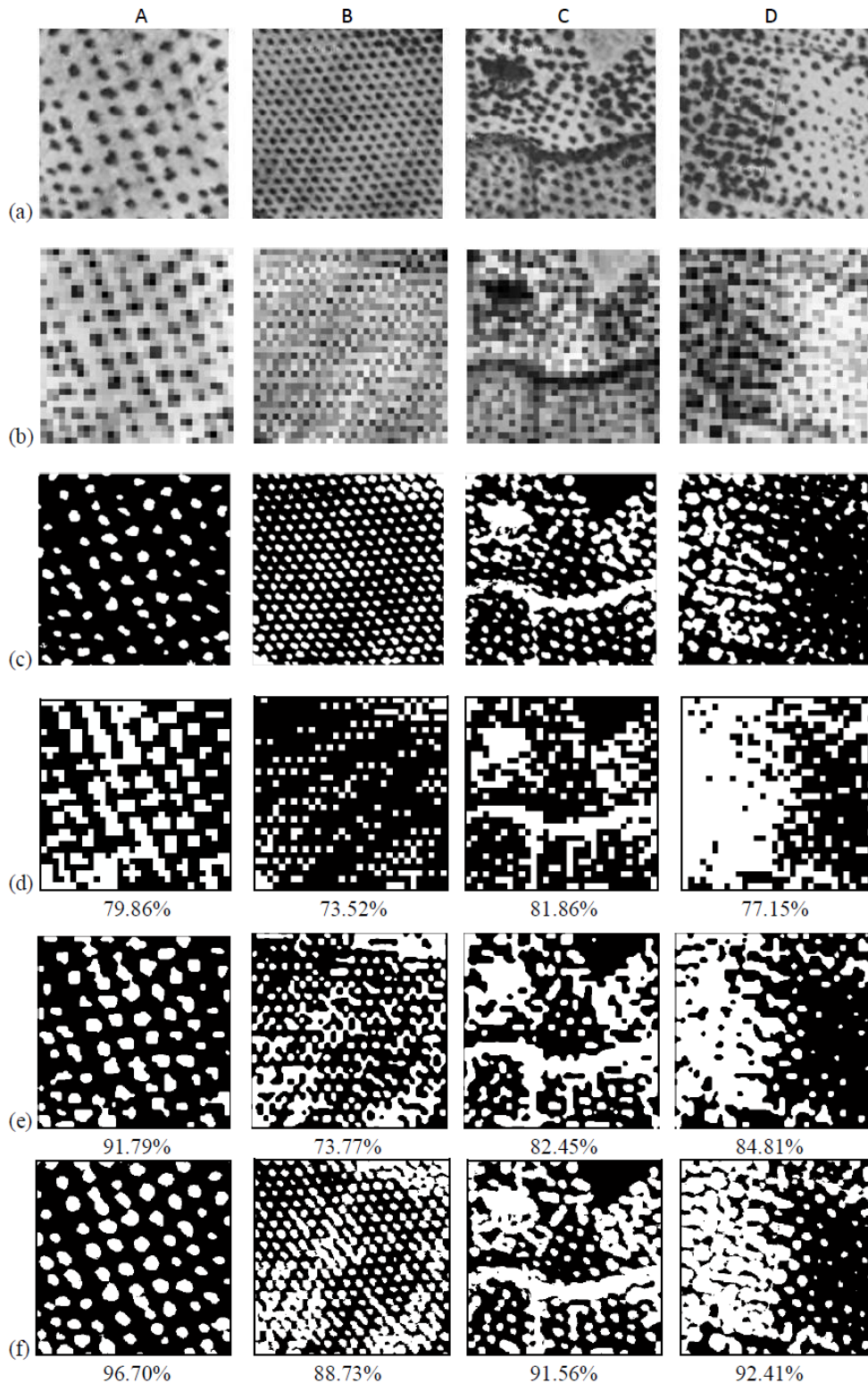
Figure 1. Mapping four landscapes, A-D. (a) Original images, each 256 × 256 pixels, (b) Spatially degraded images, each degraded by a factor of 8 and 32 × 32 pixels, (c) Hard classification of the original imagery used as reference data for the evaluation of maps derived from the degraded imagery, (d) Hard classification of the degraded imagery, (e) Super-resolution maps from the standard HNN and (f) Super-resolution maps from the HNN using prior information on landscape pattern. The overall accuracy, expressed as percentage correct allocation, is listed below each map derived from the degraded data.

(a)

(b)

(c)

(d)

(e)
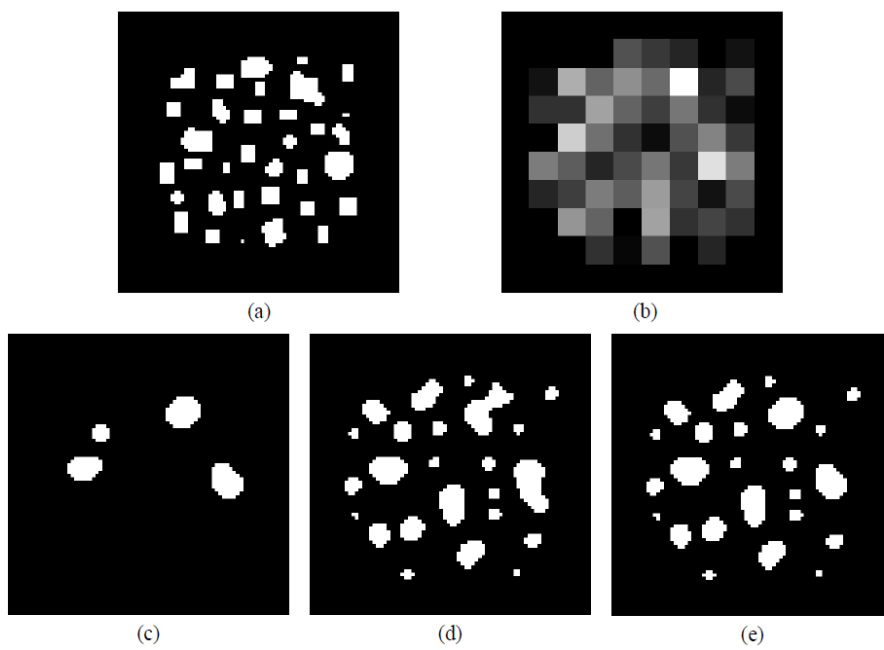
Figure 2. Patch mapping. (a) Simulated image, (b) Spatially degraded image used as soft classification for input to super-resolution analyses, (c) Output from HNN(E), (d) Output from HNN(A), (f) Output from HNN2.
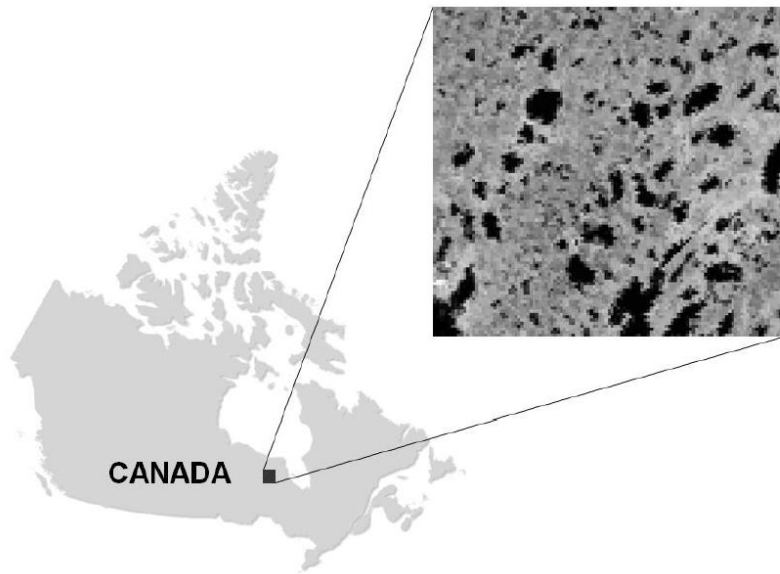
Figure 3. Location of test site and MODIS image.

(a)   (b)   (c)
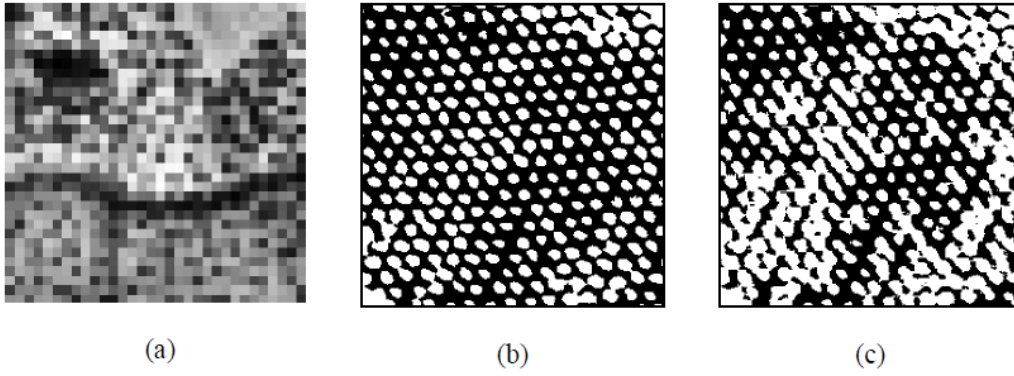
Figure 4. Importance of using appropriate prior information. (a) Image of landscape C, (b) prior information derived for landscape B, (c) output from HNN using prior information applied to the degraded image of landscape C (see Figure 1b).
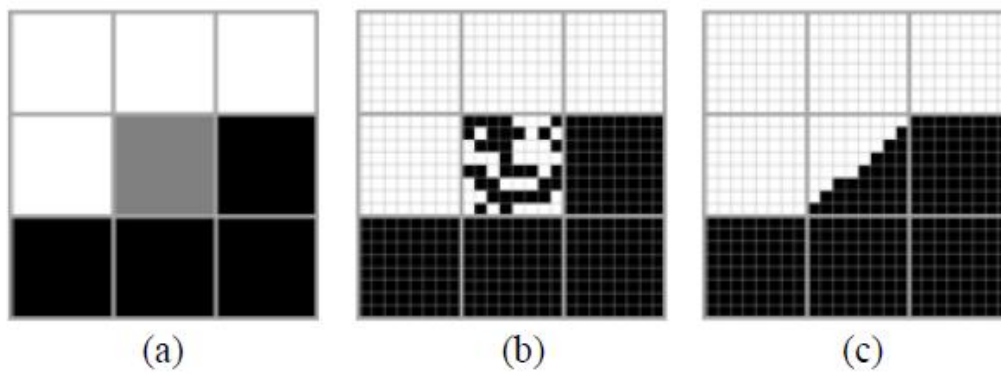
Figure 5. Super-resolution mapping when a patch is large. (a) 3×3 block of coarse pixels, all are pure except the central pixel for which the class proportion =0.5, (b) initial random allocation of sub-pixels in a HNN-based analysis, (c) Output of the HNN. The same layout is used in Figures 6-8
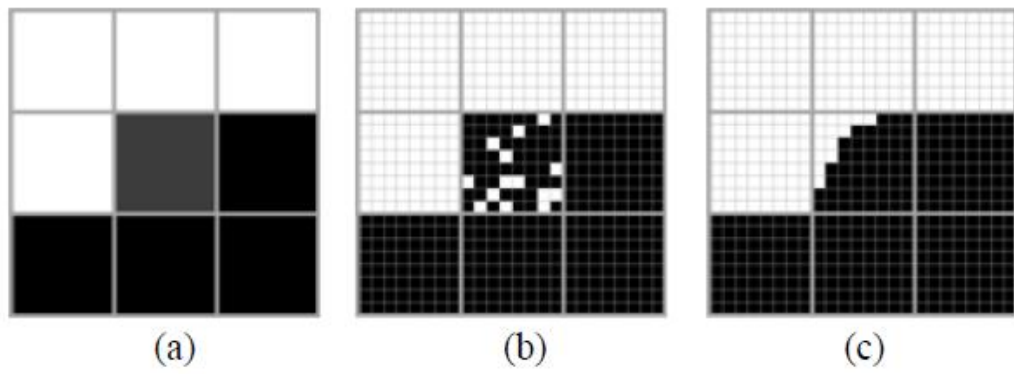
Figure 6. Super-resolution mapping when a patch is large, the class proportion of the central pixel is 0.2.
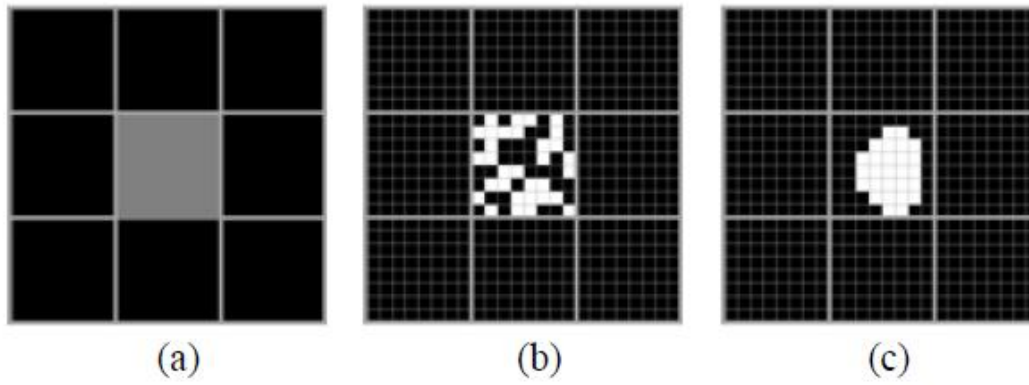
Figure 7. Super-resolution mapping when a patch is small, the class proportion of the central pixel is 0.5.
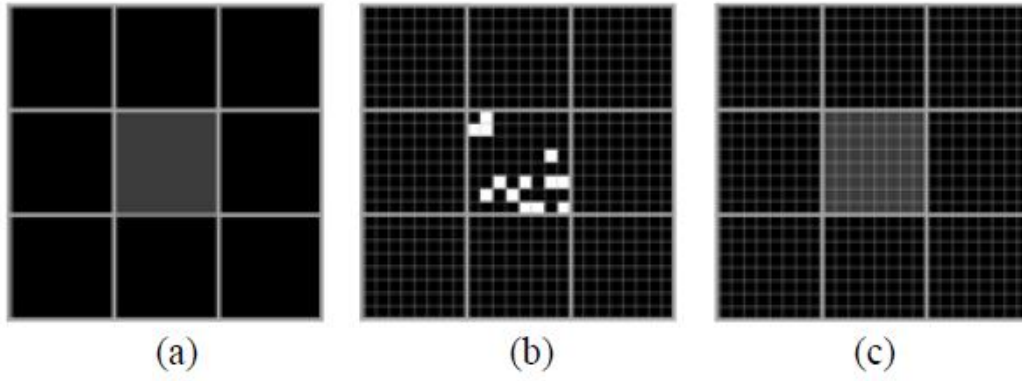
Figure 8. Super-resolution mapping when a patch is small, the class proportion of the central pixel is 0.2.
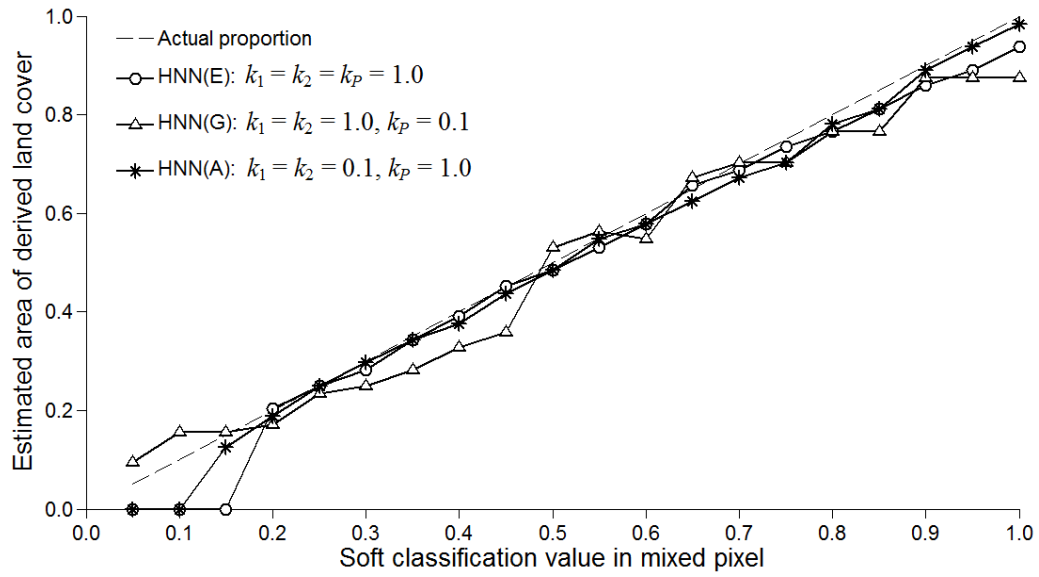
(a)
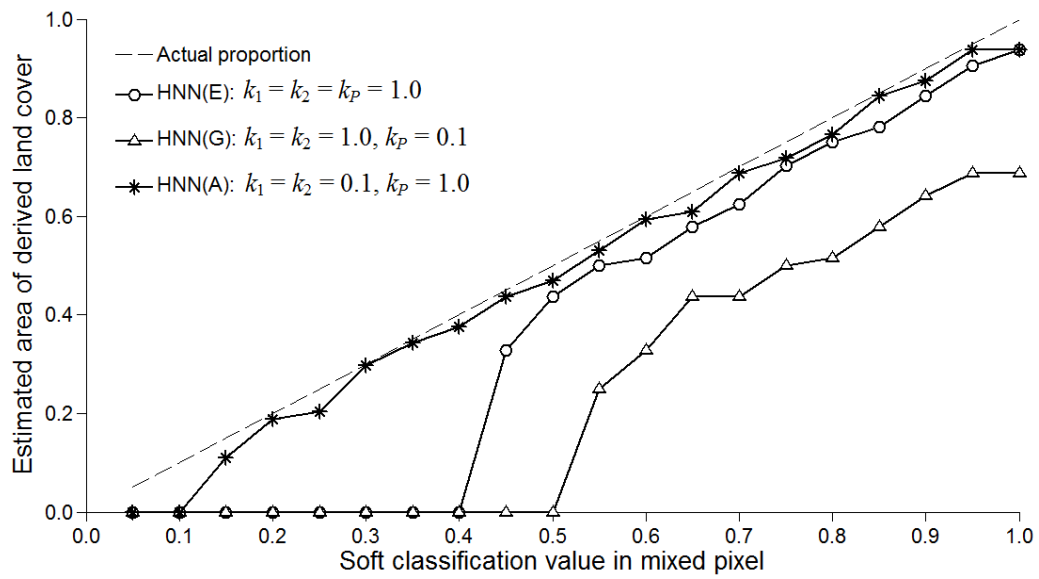
(b)

Figure 9. Relationships between the estimated patch area and the soft classification value of a mixed pixel that equated to the actual patch area from the HNN(E), HNN(G) and HNN(A) each run for 10,000 iterations. (a) large patches, (b) small patches.
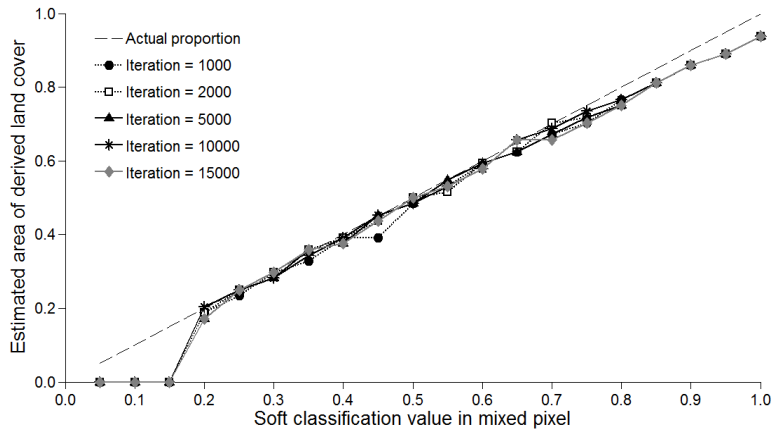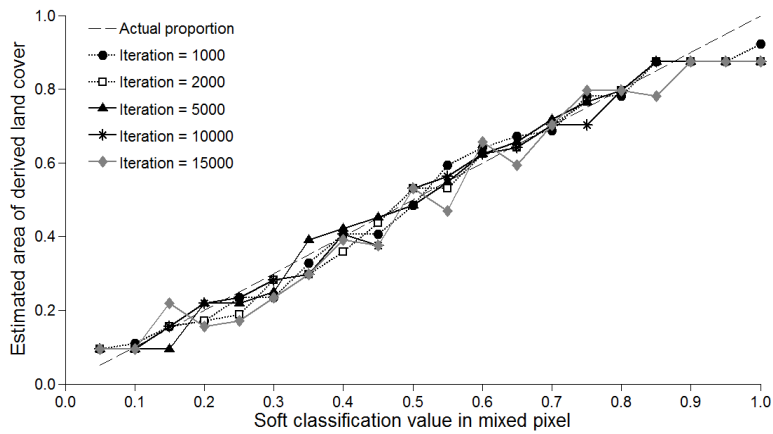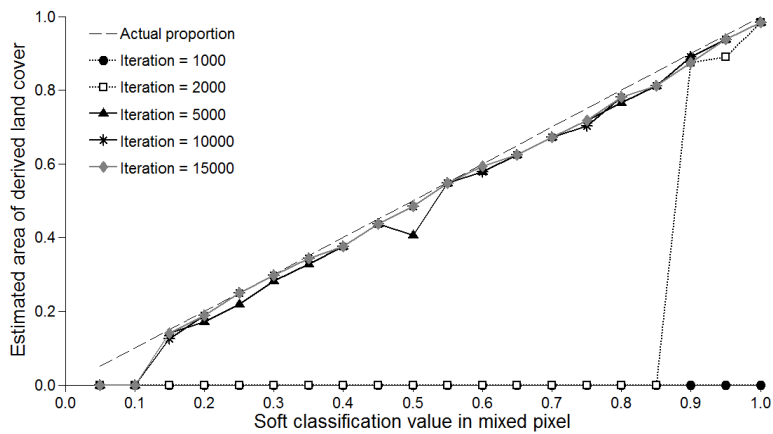
Figure 10. Relationships between the estimated patch area and the soft classification value of a mixed pixel that equated to the actual patch area for large patches. (a) HNN(E), (b) HNN(G), (c) HNN(A).
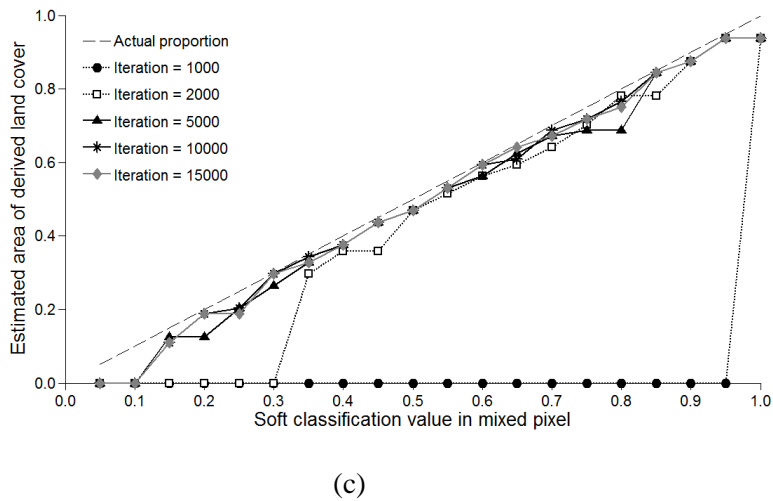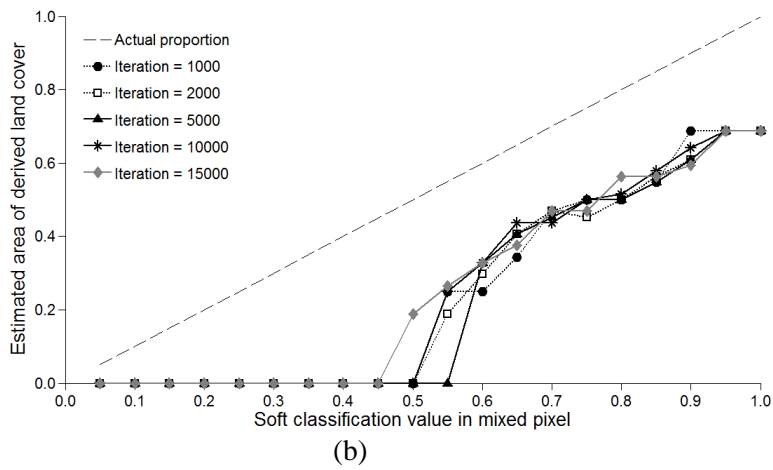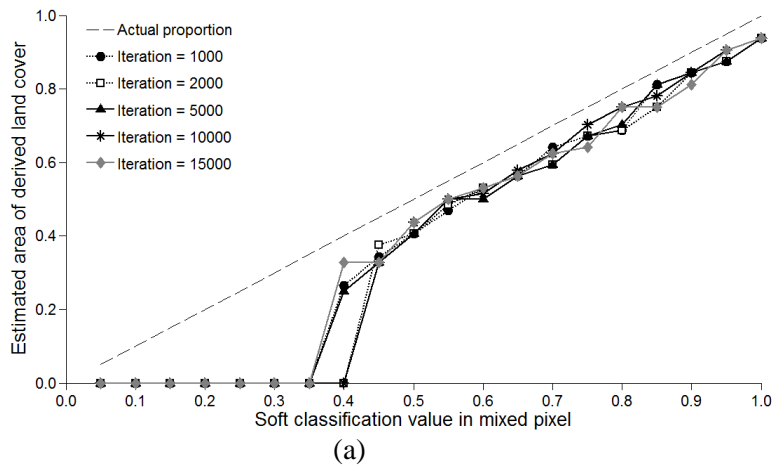
Figure 11. Relationships between the estimated patch area and the soft classification value of a mixed pixel that equated to the actual patch area for small patches. (a) HNN(E), (b) HNN(G), (c) HNN(A).
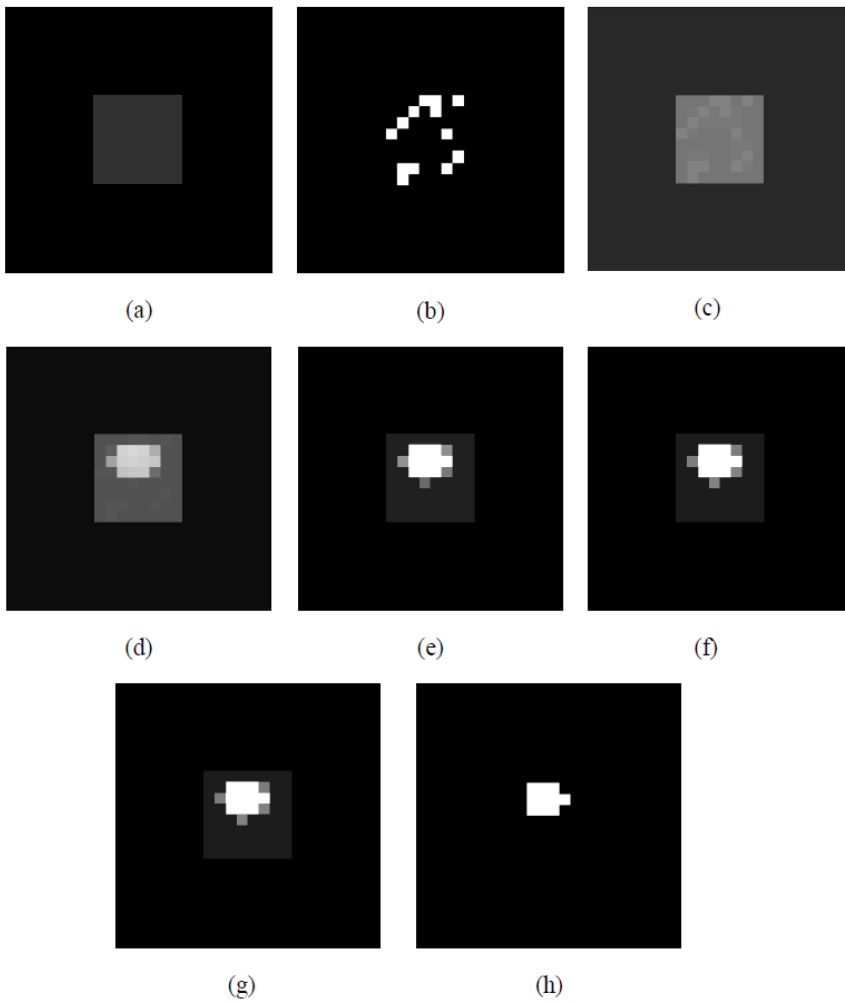
Figure 12. Example of using HNN(A). (a) Original image, soft classification value of the central pixel = 0.2, (b) Initial random distribution of sub-pixels, (c) Output after 1,000 iterations, (d) Output after 2,000 iterations, (e) Output after 5,000 iterations, (f) Output after 10,000 iterations, (g) Output after 15,000 iterations, (h) binarization of (g).
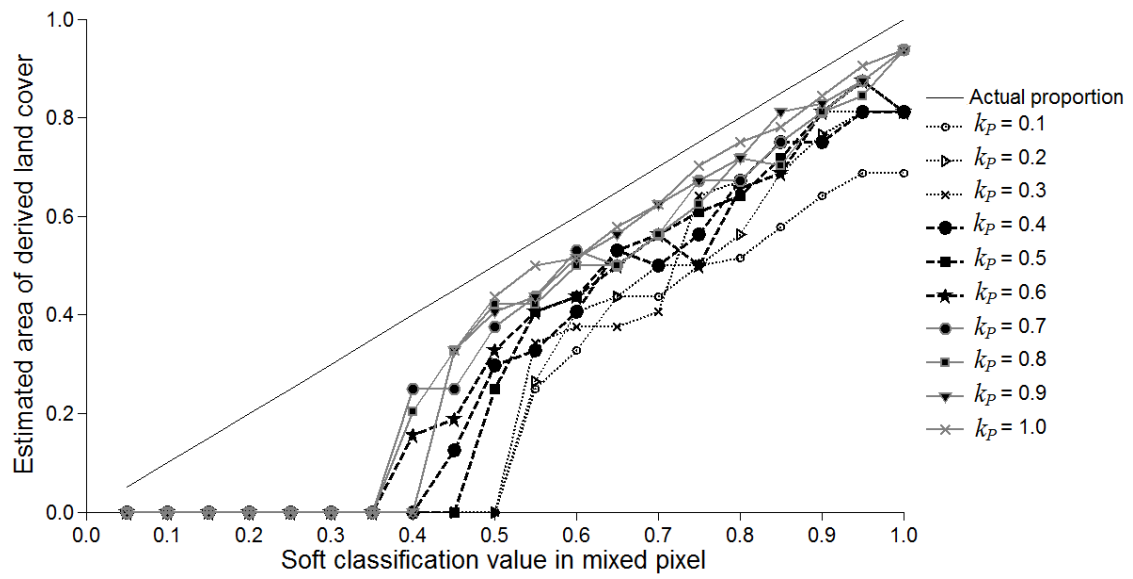
Figure 13. Relationships between the estimated patch area and the soft classification value of a mixed pixel that equated to the actual patch area for small patches at different values of k_p.
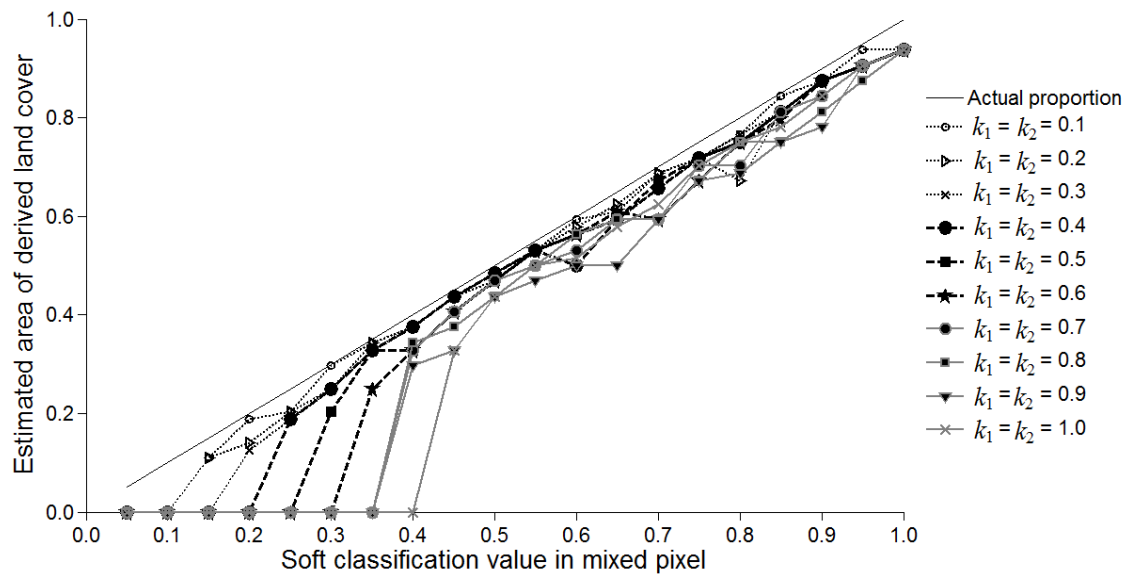
Figure 14. Relationships between the estimated patch area and the soft classification value of a mixed pixel that equated to the actual patch area for small patches at different values of $k_1=k_2$.
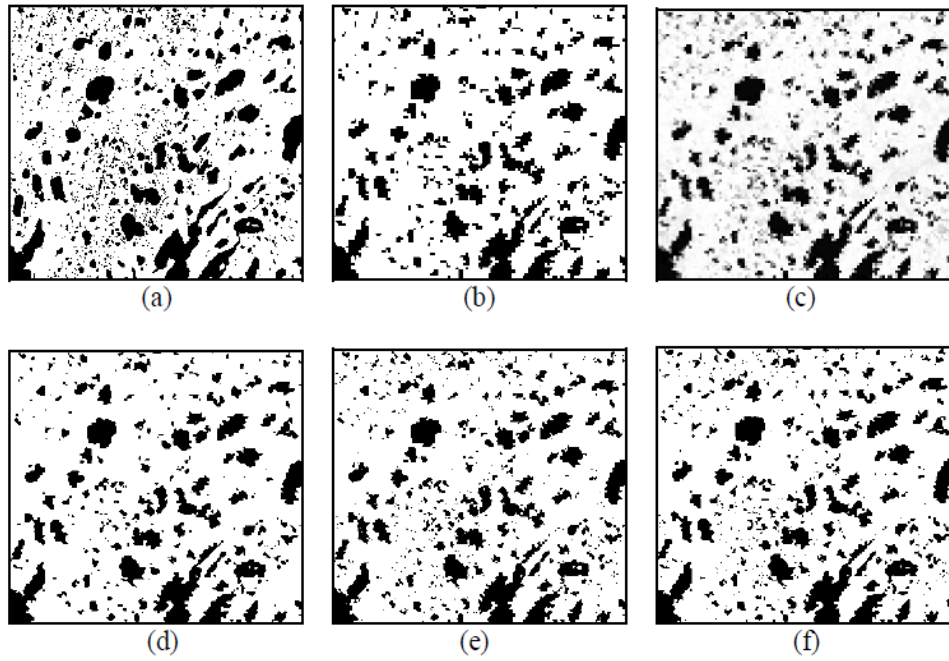
Figure 15. Analyses of the real remote sensor data. (a) Hard classification of the Landsat ETM+ data used as reference data, (b) Hard classification of the MODIS data, (c) Soft classification of the MODIS data, (d) Output of HNN(E), (e) Output of HNN(A), (f) Output of HNN2.

Author bio statements

Anuar M. Muad received the B.Eng. and M.Sc. degrees in electrical engineering from Universiti Kebangsaan Malaysia in 1999 and 2005, respectively and the Ph.D. degree in remote sensing from University of Nottingham, U.K. in 2011.

He is currently a lecturer in the Department of Electrical, Electronic and Systems Engineering, Universiti Kebangsaan Malaysia. His research interests include image and signal processing in remote sensing, computer vision and pattern recognition.

Giles M. Foody (M'01, SM'10) earned the B.Sc. and Ph.D. degrees from the University of Sheffield, U.K., in 1983 and 1986, respectively.

He is currently Professor of Geographical Information Science at the University of Nottingham, U.K. His main research interests focus on the interface between remote sensing, ecology, and informatics.

Professor Foody is currently the Editor-in-Chief of the *International Journal of Remote Sensing* and of *Remote Sensing Letters*. He holds editorial roles with *Landscape Ecology* and *Ecological Informatics* and serves on the editorial board of several other journals.